1 **Measurement report: Crustal materials play an increasing role in elevating**

2 **particle pH: Insights from 12-year records in a typical inland city of China.**

3 Hongyu Zhang[1,2], Shenbo Wang [2,3]*, Zhangsen Dong [1,2]*, Xiao Li [2,3], Ruiqin Zhang[2,3]

5 [1] Collage of Chemistry, Zhengzhou University, Zhengzhou, 450000, China

6 [2] Research Institute of Environmental Sciences, Zhengzhou University, Zhengzhou

7 450000, China

8 [3] School of Ecology and Environment, Zhengzhou University, Zhengzhou, 450000,

9 China

11 ***** Corresponding authors: Shenbo Wang and Zhangsen Dong

12 E-mail address: shbwang@zzu.edu.cn and dzszzu1990@163.com

Abstract

15 Particle acidity is a critical parameter that affects atmospheric chemistry. Concerns have been

16 raised about the exacerbating aerosol and rainfall acidity due to China's ongoing efforts to reduce

17 ammonia emissions. Therefore, it is urgent to clarify the changing trends in particle pH response to air

18 pollution control policies, especially in North China, which is significantly affected by dust aerosol.

19 12-years observational data in Zhengzhou reveal that the annual average $PM_{2.5}$ concentration

20 decreased from 212 ± 102 μg/m^3 in 2013 to 60 ± 41 μg/m^3 in 2022, with the largest reduction in sulfate

21 (79%). Correspondingly, the annual particle pH increased by 0.11 units from 2013 to 2019. In addition,

22 the elevated particle pH in 2015 and 2018 was notably influenced by the increase in TNH_x (NH_3 +

23 NH_4^+). Note that the crustal material concentrations and their proportions increased significantly

24 during 2019–2022, which might be responsible for the resuspension of surrounding soil dust. Even

25 though the TNH_x concentration was decreasing, the annual average growth rate of pH values increased

26 to 0.21 units from 2019 to 2022. This phenomenon is not unique to Zhengzhou, as major cities in the

27 North China Plain have also experienced a pronounced upward trend in coarse particles after 2019.

28 Therefore, the future ammonia reduction policies in North China may not lead to a rapid increase in

29 particle acidity buffering by the crustal materials.

30 **Keywords:** Dust, aerosol acidity, sources, North China Plain, control measurement

32 **Synopsis:** The future ammonia reduction policies in North China may not lead to a rapid increase in

33 particle acidity in the presence of crustal materials., which further elevated the particle pH after 2019.

34 **Graphical abstract:**
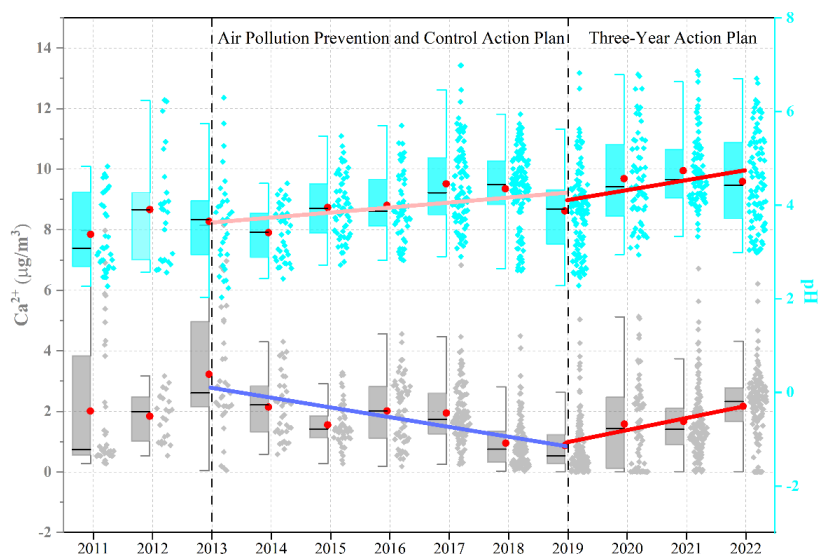
35

36

37

38 **Highlights:**

39 • Crustal material concentrations and their proportions increased significantly during 2019–2022;

40 • The resuspension of surrounding soil dust may determine the rebound of crustal material

41   concentrations;

42 • Rebound in crustal material further elevated the particle pH.

43

1 Introduction

44

45   Particle acidity is a critical parameter that affects atmospheric chemistry, such as the gas-particle

46   partitioning of semi-volatile and volatile species (Surratt et al., 2010; Guo et al., 2016), the solubility

47   of metals (Tao and Murphy, 2019), acid-catalyzed reactions (Rengarajan et al., 2011), and acid

48   deposition (Mao et al., 2009), thereby determining aerosol concentration and chemical composition,

49   as well as impacting human health, ecosystems, and climate (Li et al., 2017; Pye et al., 2020; Su et al.,

50   2020; Nenes et al., 2021). Generally, the global fine particulate matter (PM$_{2.5}$, aerodynamic diameter

51   ≤ 2.5 μm) exhibits a bimodal pH distribution ranging from 1–3 (e.g., in the United States and Europe)

52   (Guo et al., 2015; Battaglia et al., 2017; Masiol et al., 2020; Zhang et al., 2021) and 4–5 (e.g., in East

53   Asia) (Kim et al., 2022; Sharma et al., 2022). The atmosphere rich in gaseous ammonia (NH$_3$) and

54   crustal material (CM) shows significant pH buffering effects (Wang et al., 2020; Zheng et al., 2020;

55   Karydis et al., 2021), which is a dominant factor that drives the high particle pH in East Asia (Karydis

56   et al., 2021; Zhang et al., 2021; Kim et al., 2022; Sharma et al., 2022).

57   In recent years, the changing trends in particle pH have become a research hotspot, especially in

58   China, in response to air pollution control policies, i.e. Air Pollution Prevention and Control Action

59   Plan (2013–2018) and Three-Year Action Plan (2018–2020). The annual average PM$_{2.5}$ concentration

60   in Beijing dropped by 64% from 89.5 μg/m³ in 2013 to 32 μg/m³ in 2023 (MEP, 2023), with a clear

61   downward trend of sulfate concentration, and nitrate surpassing sulfate as the primary component

62   (Zhai et al., 2019; Zhou et al., 2019; Li et al., 2023). In contrast, the NH$_3$ predominantly originates

63   from agricultural activities, whose concentration has been relatively steady. These patterns have

64   fostered a persistent belief that aerosols will tend to become increasingly neutral, transitioning the

65   inorganic aerosol composition from ammonium sulfate to ammonium nitrate (Pinder et al., 2007, 2008;

66   Heald et al., 2012; Weber et al., 2016). For instance, a significant increase in the nitrate-to-sulfate

67   molar ratio from 2014–2017 in Beijing resulted in the particle pH increasing from 4.4 to 5.4 (Xie et

68   al., 2020). Moreover, increased NH_3 concentrations raised particle pH by 0.3–0.4 units from 2014/2015

69   to 2018/2019 in Beijing (Song et al., 2019). Over Europe and North America, the pH has increased

70   strongly from about 2.8 and 2.2 during the 1970s to 3.9 and 3.3 in 2020 respectively, especially during

71   the 1990s, with significantly increasing NH_3 emission (Karydis et al., 2021). On the contrary, modeling

72   results indicate a continuous decline in pH in East Asia from 1970 to 2020 due to sharp increases in

73   SO_2 and NO_x emissions (Karydis et al., 2021). In addition, the $PM_{2.5}$ pH showed a slight decrease of

74   0.13 from 2018 to 2022 summer in Beijing due to the change in total nitrate ($NO_3^- + HNO_3$) (Li et al.,

75   2023). Moreover, Zhou et al. (2022) found a decreasing pH trend from 2011 to 2019 in eastern China,

76   primarily influenced by temperature, followed by sulfate and non-volatile cations. Similarly, Nah et al.

77   (2023) observed a decreasing pH trend from 2011 to 2020 in Hong Kong, attributing it to temperature

78   and sulfate levels. Thus, concerns have been raised about the potential increase in the acidity of aerosol

79   and precipitation due to China's ongoing efforts to reduce ammonia emissions, which pose severe

80   health risks and acid deposition (Liu et al., 2019; Shi al., 2019).

81   In addition to NH_3, CM is another key alkaline substance, that buffers particle pH. Ca^{2+} can form

82   insoluble $CaSO_4$ with sulfate, reducing sulfate concentration in the aqueous phase of aerosol, and thus

83   lowering H^+ and aerosol liquid water content (ALWC) concentrations and enhancing particle pH (Ding

84   et al., 2019; Karydis et al., 2021). Moreover, non-volatile cations can lower the molar ratio of ammonia

85   to sulfate, leading to an increase in particle pH (Zheng et al., 2022). Karydis et al. (2021) simulated

86   that CM directly increased aerosol pH from 4 to 7 in the Middle East. Wang et al. (2022) reported that

87   non-volatile cations accounted for approximately 8–17% of hourly aerosol pH variation. Li et al. (2023)

88   indicated that the buffering effect of cations was the major reason for the relatively small pH changes

89   from 2018 to 2022 in Beijing, emphasizing that reducing coarse particle emissions in the future could

90   significantly decrease particle pH. In addition, there was a rising trend in the contribution of CM to

91   particle pH in Tianjin, China (Shi et al., 2017). Therefore, it is evident that CM has a significant impact

92   on the variation of particle pH, especially in North China, which is significantly affected by dust

93   aerosol, but the trend of CM concentration and its long-term implication is still lacking unfortunately.

94   2 Experiment and method

95   2.1 Instruments and Measurements

96   Sampling was conducted on the fourth-floor platform at Zhengzhou University (34.75° N, 113.61°

97   E) in Zhengzhou, China. The sampling site (Fig. S1), approximately 14 m above the ground, is

98   primarily surrounded by residential areas with well-developed transportation networks and no

99   significant industrial sources. There are two highways located 3 km to the south and 7 km to the east.

100   Additionally, a coal-fired power plant located 6 km to the east was shut down in 2020, and a gas-fired

101   power plant is situated 3 km to the south.

102   Samples were collected using a high-volume sampler (TE-6070D, Tisch, USA) and air particulate

103   samplers (TH-16A, Tianhong, China) from April 2011 to December 2022. Two quartz filters and two

104   Teflon filters were used daily from 10:00 AM to 9:00 AM the next day, resulting in a total of 5848

105   samples. After excluding abnormal data due to instrument malfunctions, 4228 valid samples were

106   obtained. Detailed information on the samples is provided in Table S1. Organic carbon (OC) and

107   elemental carbon (EC) were analyzed using a carbon analyzer (Model 5L, Sunset Laboratory, USA).

108   Water-soluble inorganic ions (Cl^-, NO_3^-, SO_4^{2-}, Na^+, NH_4^+, K^+, Mg^{2+}, and Ca^{2+}) were measured using

109   ion chromatography (ICS-90 and ICS-900 models, Dionex, USA) (Yu et al., 2017; Jiang et al., 2018).

110   Elements were analyzed using a wavelength dispersive X-ray fluorescence spectrometer (S8 TIGER,

111   Bruker, Germany) to determine concentrations of Fe, Na, Mg, Al, Si, P, S, Cl, K, Ca, Ti, V, Ni, Cu, Zn,

112   Cr, Mn, Co, Ga, As, Se, Sr, Sn, Sb, Ba, and Pb (Tremper et al., 2018). Meteorological conditions,

113   including temperature (T), relative humidity (RH), and wind speed (WS) were obtained using an

114   automatic weather station (Wang et al., 2019). Detailed analytical methods and quality control are

115   described in Refs (Jiang et al., 2018; Yang et al., 2020).

116   **2.2 Data Analysis**

117   **2.2.1 Mass reconstruction**

118   The calculation method for CM is as follows (Tian et al., 2016):

119                   $$[CM]=1.89\times[Al] + 2.14\times[Si] + 1.4\times[Ca] + 1.43\times[Fe] \qquad (1)$$

120   where [Al], [Si], [Ca], [Fe] and [Ti] represent the concentrations of the respective elements ($\mu g/m^3$),

121   but Ti was not measured.

122   **2.2.2 Thermodynamic model**

123   The particle pH was calculated using the ISORROPIA-II model (http://isorropia.eas.gatech.edu).

124   Input data (excluding RH ≤ 30%) included SO_4^{2-}, TNO_3 ($HNO_3 + NO_3^-$), TNH_x ($NH_3+NH_4^+$), Ca^{2+},

125   K^+, Na^+, Mg^{2+}, Cl^-, RH and T. The concentrations of hydrogen ions in air (H_{air}^+) and ALWC were

126   calculated using the aerosol equilibrium composition system Na^+-K^+-Ca^{2+}-Mg^{2+}-NH_4^+-SO_4^{2-}-NO_3^--

127   Cl^--H_2O H_{air}^+ (Fountoukis and Nenes, 2007). pH values were calculated using the following formula:

128
$$pH = -\log_{10} H_{aq}^+ \cong -\log_{10} \frac{1000 H_{air}^+}{ALWC_i + ALWC_o} \cong -\log_{10} \frac{1000 H_{air}^+}{ALWC_i} \qquad (2)$$

129
$$ALWC_o = \frac{m_{org} \rho_w}{\rho_w} \frac{\kappa_{org}}{\left(\dfrac{1}{RH} - 1\right)} \qquad (3)$$

130   where $ALWC_i$ and $ALWC_o$ refer to the ALWC for inorganic and organic components, respectively.

131   m_{org} denotes the mass of organic aerosol, ρ_w is the density of water (1.0 g/cm^3), ρ_{org} is the density of

132   organic material (1.4 g/cm^3) (Guo et al., 2015), k_{org} is the hygroscopicity parameter for organic aerosol

133   (0.087) (Chang et al., 2010; Li et al., 2016). The ISORROPIA-II model operated under metastable

134   conditions in the forward mode. Due to the lack of measured data for gaseous HNO_3 and NH_3, TNO_3

135   was represented solely by NO_3^-. The concentration of NH_3 was simulated based on a linear regression

136   equation proposed by Wei et al. (2023), who used the same data as this study from 2013 to 2020:

137    $$NH_3 = 19.909 \times RH + 0.559 \times T - 0.35 \times NH_4 + 0.123 \times NO_3^- + 2.159 \times Cl^- - 0.224 \times SO_4^{2-} - 154.923 \quad (4)$$

138   where NO_3^-, SO_4^{2-}, NH_4^+, and Cl^- correspond to their respective concentrations (μg/m^3).

2.2.3 HYSPLIT analysis

Backward trajectories were calculated using the mixed-particle Lagrangian integrated trajectory method (HYSPLIT, https:// www.ready.noaa.gov/HYSPLIT_traj.php). 24-h backward trajectories were simulated for air masses above 1000 m above ground level in Zhengzhou. Subsequently, trajectories from two periods, 2013–2018 and 2019–2022, were clustered separately to analyze the variations between the two policy implementation periods.

3 Results and discussion

3.1 Temporal variations in chemical components

The long-term trends in $PM_{2.5}$ concentrations and its chemical components from 2011 to 2022 are depicted in Fig. 1, with annual average concentrations listed in Table 1. Over the past twelve years, the Chinese government implemented the Air Pollution Prevention and Control Action Plans (2013–2018) and the Three-Year Action Plan (2018–2020), gradually improving air quality in Zhengzhou. The annual average concentration of $PM_{2.5}$ decreased from 212 ± 102 µg/m^3 in 2013 to 60 ± 41 µg/m^3 in 2022, representing a reduction of approximately 72%. As for chemical components, the largest reductions were observed in SO_4^{2-} (79%), decreasing from 38.0 ± 19.9 µg/m^3 in 2013 to 7.9 ± 4.5 µg/m^3 in 2022, followed by EC (76%). Additionally, the concentrations of NH_4^+ and NO_3^- also significantly decreased by 68% and 56%, respectively. The proportion of each component in $PM_{2.5}$ (Fig. S2) reveals a decrease in SO_4^{2-}, K^+, and Cl^-, indicating effective control measures targeting coal and biomass combustion (Lei et al., 2021). However, the proportions of NO_3^- and OC in $PM_{2.5}$ rose

158   from 11% and 12% in 2013 to 13% and 17% in 2022, respectively, similar to the trend observed in the

159   North China Plain (Wen et al., 2018; Zhai et al., 2019; Li et al., 2023).

3.2 Temporal variations in CM

161   Notably, there is no clear declining trend in the CM concentration, with a rebound observed during

162   2020–2022 (Fig. 1i). Furthermore, the proportion of CM in $PM_{2.5}$ exhibits a significant upward trend

163   (Fig. S2). To further analyze its trend, sampling data were divided into three periods corresponding to

164   governmental stages: 2011–2013, when no special control measures were implemented; 2013–2019,

165   coinciding with the implementation of the Air Pollution Prevention and Control Action Plan; and

166   2019–2022, coinciding with the Three-Year Action Plan. During these periods, Henan Province and

167   Zhengzhou City implemented several dust control policies summarized in Table S2. As shown in Fig.

168   2a and 2b, the mass concentration of CM peaked at 14.6 ± 8.3 μg/m^3 in 2013, accounting for 8% of

169    $PM_{2.5}$. From 2013 to 2019, the CM concentration notably decreased from 14.6 ± 8.3 to 8.5 ± 7.8 μg/m^3,

170   with an annual average decline rate of 0.81 μg/(m^3·year). Seasonal trends (Fig. S3) indicate more

171   pronounced decreases in spring and summer compared to autumn and winter, possibly due to favorable

172   meteorological conditions such as higher WS promoting dust resuspension, where conventional dust

173   control measures (e.g., road sprinkling, sealed transport vehicles, and covering large piles) were more

174   effective. In autumn and winter with low WS, dust sources were likely dominated by primary releases,

175   such as demolition dust, which have no significant regulatory measures. (Wang et al., 2013, 2018). As

176   for the individual crustal elements in Fig. S4, Ca exhibited the highest average annual decline rate of

177   33% during 2013–2019, followed by Al. Si showed a less pronounced decline, attributed to its

178   association with soil dust, where control measures for exposed soil are lacking (Zhang et al., 2020). In

179   addition, the Ca^{2+} concentration as depicted in Fig. 2c decreased from 3.2 ± 2.1 μg/m^3 in 2013 to 2.2

180   ± 1.1 μg/m^3 in 2019, with an approximate annual average decline rate of 0.3 μg/(m^3·year), further

181   demonstrating the decline in dust source. Apart from control measures, WS exhibited a declining trend

182   (Fig. S5), with a decrease rate of 43%, while RH showed an increasing trend at a rate of 8% from 2013

183   to 2019, under which conditions that were unfavorable for dust resuspension (Wang et al., 2013, 2018).

184   It was worth noting that the proportions of CM, Ca, Al, Fe, Si, and Ca^{2+} in PM$_{2.5}$ have shown

185   consecutive annual increases from 2013 to 2019, with CM proportion increasing from 8% in 2013 to

186   14% in 2019, indicating that CM reduction lagged behind PM$_{2.5}$ reduction efforts in Zhengzhou during

187   this period. Additionally, both concentration and proportion of Ca^{2+} in 2022 (2.2 ± 1.1 μg/m^3 and 14%)

188   were higher than in other cities of China, such as Beijing (1.0 μg/m^3 and 2.8%), Tianjin (0.5 μg/m^3 and

189   1.4%), and Xiamen (0.48 μg/m^3 and 1.5%) (Shi et al., 2017; Xu et al., 2025; Zhang et al., 2021). These

190   results indicate that CM remained an important component of PM$_{2.5}$ in Zhengzhou City.

191   During 2019–2022, both CM and Ca^{2+} concentrations exhibited significant rebounds, with annual

192   growth rates of 0.24 and 0.4 μg/(m^3·year), respectively, and their proportions increased from 14% and

193   2% in 2019 to 22% and 5% in 2022. CM concentrations rebounded in all seasons, particularly in winter

194   (Fig. S3). Changes in meteorological conditions may be a significant factor contributing to these

195   concentration rebounds, accompanied by the average WS increased by 0.14 m/s and RH decreased by

196   7% from 2020 to 2022 (Fig. S5), facilitating dust resuspension. Furthermore, the lack of more effective

197   dust control measures, as indicated by the absence of significant changes in the dust control policies

198   from the Air Pollution Prevention and Control Action Plan and Three-Year Action Plan, may be another

199   important factor contributing to the rebound of dust.

3.3 Sources of CM

201   Elemental ratios were employed to characterize the sources of CM, with the Ca/Al ratio widely

202   recognized as a reliable indicator of sandy origin (Zhang et al., 2017). In addition, significant variations

203   in Ca/Si ratios (Table S3) were observed among different dust sources (Road, Construction, Piles, Soil).

204   Fig. 3a illustrates the trend in Ca/Si ratios from 2011 to 2022. After 2013, Ca/Si ratios showed a

205   declining trend annually, with the average ratio decreasing from a peak of 1.6 in 2016 to a lowest of

206   0.4 in 2022. Compared with Ca/Si ratios from different types of dust sources, the effect of road and

207   construction dust on CM has gradually decreased. This may be attributed to the implementation of dust

208   control measures such as enclosure, shielding, and dust suppression at construction and demolition

209   sites, as well as dust control on ground surfaces and roads (Table S3). During 2019–2022, the average

210   Ca/Si ratio remained below 1, with a mean of 0.4 in 2022, indicating that soil dust predominantly

211   contributed to CM. Currently, measures for controlling soil-suspended dust are limited, primarily

212   relying on long-term strategies such as afforestation and increasing urban green coverage, thus

213   requiring a longer process and sustained investment.

214   Sand dust transport serves as a significant source of CM in the North China Plain (Zhang et al.,

215   2024). The Ca/Al ratio from 2016 to 2022 (Fig. 3b) shows minimal variation, with annual averages

216   ranging between 1.5 and 2.5, indicating no significant changes in the source regions of sand. The

217   transport trajectories reveal that the predominant pathways for long-distance transport of sand dust

218   originated from Inner Mongolia, passing through Shaanxi and Shanxi provinces. Compared to 2013–

219   2018 (45%), the influence of long-distance transport decreased to 25% during 2019–2022. In contrast,

220   local transport within Henan province and short-distance transport from Shandong province showed a

221   noticeable increase. These findings suggest that the rebound in CM concentrations during 2019–2022

222   in Zhengzhou might be responsible for the resuspension of surrounding soil dust.

223   **3.4 Long-term trend of particle pH**

224   Are shown in Fig. 4, pH values showed a clearly increasing trend after 2014. From 2013 to 2019,

225   the annual pH increased by 0.11 units, reaching a maximum median value of 4.45 (Mean: 4.35) in

226   2018. Note that the annual average growth rate of pH values increased to 0.21 units from 2019 to 2022,

227   with a maximum median value of 4.42 (Mean: 4.51) in 2022. Seasonally, pH values showed increasing

228   trends in spring, summer, and autumn, and notably increased in winter from 2020 to 2022 (Fig. S6).

229   The increasing trend in pH values observed in this study is similar to the findings in Beijing (Song et

230   al., 2019; Xie et al., 2020), but differs from those reported in Shanghai and Hong Kong (Nah et al.,

231   2023; Zhou et al., 2022).

232   Sensitivity analyses were conducted to explore the dominant factors driving the elevated particle

233   pH in Zhengzhou by giving a range for one parameter and average values for other parameters input

234   into the ISORROPIA-II model. Are shown in Fig. S7, particle pH increases with the cation

235   concentrations (e.g., TNH_x, K^+, Ca^{2+}, Mg^{2+}, and Na^+) and decreases with anions concentrations (e.g.,

236   SO_4^{2-} and NO_3^-). Additionally, RH does not significantly affect pH, whereas an increase in T leads to

237   a noticeable decrease in particle pH.

238   The changes in pH (ΔpH) between adjacent years are illustrated in Fig. 5, with the differences in

239   influencing factors listed in Table S4. Obviously, the decline in SO_4^{2-} from 2013 to 2018 was the

240   primary cause of the increase in particle pH, as it decreased H^+ and ALWC concentrations (Fig. S8) in

241   aerosol (Ding et al., 2019; Zhang et al., 2021). The average SO_4^{2-} concentration decreased by 14.6 and

242   5.3 μg/m^3, resulting in a pH increase of 0.43 and 0.35 units from 2013 to 2014 and 2016 to 2017,

243   respectively, which was comparable to an increased rate of 0.3 units in East Asia due to SO_2 emission

244   controls since 2016 (Karydis et al., 2021). As another acidic ion, the decrease in nitrate concentration

245   did not significantly contribute to the pH increases, consistent with findings from Ding et al. (2019)

246   and Zhang et al. (2021). This is primarily because nitrate ions decline more slowly compared to sulfate

247   ions and exceeded sulfate concentrations after 2016, under which conditions that nitrate-rich particles

248   can absorb twice the amount of water that sulfate-rich particles, leading to an increase in ALWC

249   concentration and inhibiting pH decline (Lin et al., 2020; Xie et al., 2020). On the other hand, increases

250   in particle pH in 2015 and 2018 were notably influenced by changes in TNHx with concentrations

251   increased by 5.5 and 1.3 μg/m^3, respectively. Increased TNH_x concentrations could react with SO_4^{2-}

252   /NO_3^- and consume a substantial amount of H^+, thereby raising particulate matter pH values (Seinfeld

253   et al., 1998; Zhang et al., 2021). Substantial decreases in T in 2015 (4.2℃), 2017 (4.9℃), and 2018

254   (2.8℃), favoring NH_3 partitioning into the particle phase and reducing H^+ concentrations, drove

255   increases in particle pH (Tao and Murphy, 2019).

256   During the period from 2020 to 2022, the influence of SO_4^{2-} on particle pH gradually decreased,

257   with a decrease in concentration from 0.3 to 2.3 μg/m^3 only bringing about a pH decrease of 0.03 to

258   0.14. Moreover, a rebound in SO_4^{2-} concentration to 7.9 ± 4.5 μg/m^3 in 2022 even resulted in a decrease

259   of 0.11 units in pH instead. On the other hand, TNHx began to show a slight annual decline (0.9 to 2.2

260   μg/m³), resulting in a significant decrease in pH (0.21–0.35). Consequently, the increase in pH values

261   was closely related to the rise in Ca^{2+} concentration. Ca^{2+} is less volatile and competes preferentially

262   with NH_3 to neutralize anions such as SO_4^{2-} to form insoluble $CaSO_4$, which precipitates from the

263   aerosol aqueous phase (Ding et al., 2019; Karydis et al., 2021), thereby reducing H^+ concentrations

264   (Fig. S8) and subsequently lowering particle acidity. Specifically, increases of 0.7 and 0.5 μg/m³ in

265   Ca^{2+} concentrations led to pH increases of 0.13 and 0.09 units in 2020 and 2022, respectively, making

266   Ca^{2+} a primary controlling factor for pH elevation.

4 Conclusions

268   The annual average $PM_{2.5}$ concentration in Zhengzhou decreased from 212.4 ± 101.5 μg/m³ in

269   2013 to 59.5 ± 41.2 μg/m³ in 2022, with the largest reduction in SO_4^{2-}. As for CM, their concentrations

270   notably decreased from 2013 to 2019, because of effective dust control measures, as well as decreased

271   wind speed and increased relative humidity. However, the proportions of CM in $PM_{2.5}$ have shown

272   consecutive annual increases. In addition, CM concentrations and their proportions increased

273   significantly during 2019–2022, which might be responsible for the resuspension of surrounding soil

274   dust. Correspondingly, the annual pH increased by 0.11 units from 2013 to 2019 mainly due to the

275   decline in SO_4^{2-}, increased TNH_x, or decreased temperature. During the period from 2020 to 2022, the

276   annual average growth rate of pH values increased to 0.21 units from 2019 to 2022, which was

277   determined by the rise in Ca^{2+} concentration.

5 Implication

278

279   Control measures implemented by the Chinese government have proven effective in reducing dust,

280   but this study reveals that the crustal materials in PM$_{2.5}$ rebounded after 2019. This phenomenon is not

281   unique to Zhengzhou, as major cities in the North China Plain have also experienced a pronounced

282   upward trend in coarse particles after 2019 (Fig. S9). Thus, crustal materials remain a significant

283   component of atmospheric aerosols in North China, maintaining particle pH at higher levels. The

284   research predicted that China's next phase of reducing ammonia emissions would significantly

285   aggravate precipitation acidification, which poses severe health risks and acid deposition (Liu et al.,

286   2019; Shi et al., 2019). However, the presence of crustal material in the North China Plain, which is

287   difficult to reduce from soil dust, can play an important role as buffering substances to prevent quickly

288   rising acidity. Therefore, the future ammonia reduction policies in North China may not lead to a rapid

289   increase in particle acidity, but it is necessary to consider synergistic control with dust sources.

Data availability

290

291   All   the   data   presented   in   this   article   can   be   accessed   through

292   https://doi.org/10.5281/zenodo.14032007 (Zhang, 2024).

Supporting Information

293

294   Additional data, figures, and tables, some of which are referenced directly within the manuscript,

295   and detailed descriptions of field measurements and samples.

Author contributions

297   Shenbo Wang designed this study. Hongyu Zhang and Zhangsen Dong analyzed the data and

298   prepared the manuscript with the contributions of all coauthors. Xiao Li conducted measurements.

299   Ruiqin Zhang provided funding acquisition. All authors have read and agreed to the published version

300   of the manuscript.

Competing interests

302   The authors declare that they have no conflict of interest.

Acknowledgment

304   This work was supported by the China Postdoctoral Science Foundation (2023 M733220), the

305   Zhengzhou $PM_{2.5}$ and O_3 Collaborative Control and Monitoring Project (20220347 A), and the

306   National Key R&D Program of China No. 2017YFC0212400.

Funding Sources

308   This work was supported by the China Postdoctoral Science Foundation (2023 M733220), the

309   Zhengzhou $PM_{2.5}$ and O_3 Collaborative Control and Monitoring Project (20220347 A), and the

310   National Key Research and Development Program of China (No. 2017YFC0212400).

References

312   Battaglia, M. A.; Douglas, S.; Hennigan, C.: Effect of the urban heat island on aerosol pH, Environ.

313   Sci. Technol., 51, 13095–13103, https://doi.org/10.1021/acs.est.7b02786, 2017.

314   Chang, R. Y. W.; Slowik, J. G.; Shantz, N. C.; Vlasenko, A.; Liggio, J.; Sjostedt, S. J.; Leaitch, W. R.;

315   Abbatt, J. P. D. The hygroscopicity parameter (κ) of ambient organic aerosol at a field site subject

316   to biogenic and anthropogenic influences: relationship to degree of aerosol oxidation. Atmos.

317   Chem. Phys., 10, 5047–5064, https://doi.org/10.5194/acp-10-5047-2010, 2010.

318   Ding, J., Zhao, P., Su, J., Dong, Q., Du, X., and Zhang, Y.: Aerosol pH and its driving factors in Beijing,

319   Atmos. Chem. Phys., 19, 7939–7954, https://doi.org/10.5194/acp-19-7939-2019, 2019.

320   Fountoukis, C and Nenes, A.: ISORROPIA II: a computationally efficient thermodynamic equilibrium

321   model for K^+ - Ca^{2+} - Mg^{2+} - NH_4^+ - Na^+ - SO_4^{2-} - NO_3^- - Cl^- - H_2O aerosols, Atmos. Chem. Phys.,

322   7, 4639–4659, https://doi.org/10.5194/acp-7-4639-2007, 2007.

323   Guo, H., Sullivan, A. P., Campuzano-Jost, P., Schroder, J. C., Lopez-Hilfiker, F. D., Dibb, J. E., Jimenez,

324   J. L., Thornton, J. A., Brown, S. S., Nenes, A., and Weber, R. J.: Fine particle pH and the

325   partitioning of nitric acid during winter in the northeastern United States, J. Geophys. Res. Atmos.,

326   121, 10,355–310,376, https://doi.org/10.1002/2016JD025311, 2016.

327   Guo, H., Xu, L., Bougiatioti, A., Cerully, K. M., Capps, S. L., Hite Jr, J. R., Carlton, A. G., Lee, S. H.,

328   Bergin, M. H., Ng, N. L., Nenes, A., and Weber, R. J.: Fine-particle water and pH in the

329   southeastern United States, Atmos. Chem. Phys., 15, 5211–5228, https://doi.org/10.5194/acp-15-

330   5211-2015, 2015.

331   Heald, C.; Collett, J. J.; Lee, T.; Benedict, K.; Schwandner, F.; Li, Y.; Clarisse, L.; Hurtmans, D. R.;

332   Van, D. M.; Clerbaux, C.; Coheur, P. F., Philip, S.; Martin, R. V.; Pye, T.: Atmospheric ammonia

333   and particulate inorganic nitrogen over the United States, Atmos. Chem. Phys., 12, 10295–10312,

334   https://doi.org/10.5194/acp-12-10295-2012, 2012.

335   Jiang, N.; Duan, S.; Yu, X.; Zhang, R.; Wang, K. Comparative major components and health risks of
336   toxic elements and polycyclic aromatic hydrocarbons of $PM_{2.5}$ in winter and summer in
337   Zhengzhou: Based on three-year data. Atmos. Res., 213, 173–184,
338   https://doi.org/10.1016/j.atmosres.2018.06.008, 2018

339   Jiang, N., Li, Q., Su, F., Wang, Q., Yu, X., Kang, P., Zhang, R., and Tang, X.: Chemical characteristics
340   and source apportionment of $PM_{2.5}$ between heavily polluted days and other days in Zhengzhou,
341   China, J. Environ. Sci., 66, 188–198, https://doi.org/10.1016/j.jes.2017.05.006, 2018.

342   Karydis, V. A., Tsimpidi, A. P., Pozzer, A., and Lelieveld, J.: How alkaline compounds control
343   atmospheric aerosol particle acidity, Atmos. Chem. Phys., 21, 14983–15001,
344   https://doi.org/10.5194/acp-21-14983-2021, 2021.

345   Kim, Y., Park, O., Park, S. H., Kim, M. J., Kim, J.-J., Choi, J.-Y., Lee, D., Cho, S., and Shim, S.: $PM_{2.5}$
346   pH estimation in Seoul during the KORUS-AQ campaign using different thermodynamic models,
347   Atmos. Environ., 268, 118787, https://doi.org/10.1016/j.atmosenv.2021.118787, 2022.

348   Lei, L., Zhou, W., Chen, C., He, Y., Li, Z., Sun, J., Tang, X., Fu, P., Wang, Z., and Sun, Y.: Long-term
349   characterization of aerosol chemistry in cold season from 2013 to 2020 in Beijing, China, Environ.
350   Pollut., 268, 115952, https://doi.org/10.1016/j.envpol.2020.115952, 2021.

351   Li, C.; Hu, Y.; Chen, J.; Ma, Z.; Ye, X.; Yang, X.; Wang, L.; Wang, X.; Mellouki, A. Physiochemical
352   properties of carbonaceous aerosol from agricultural residue burning: Density, volatility, and
353   hygroscopicity. Atmos. Environ., 140, 94–105, https://doi.org/10.1016/j.atmosenv.2016.05.052,
354   2016.

355   Li, W., Xu, L., Liu, X., Zhang, J., Lin, Y., Yao, X., Gao, H., Zhang, D., Chen, J., Wang, W., Harrison,
356   R. M., Zhang, X., Shao, L., Fu, P., Nenes, A., and Shi, Z.: Air pollution-aerosol interactions
357   produce more bioavailable iron for ocean ecosystems, Sci. Adv., 3, e1601749,
358   https://doi.org/10.1126/sciadv.1601749, 2017.

359   Li, Y., Lei, L., Sun, J., Gao, Y., Wang, P., Wang, S., Zhang, Z., Du, A., Li, Z., Wang, Z., Kim, J. Y.,
360   Kim, H., Zhang, H., and Sun, Y.: Significant reductions in secondary aerosols after the Three-
361   Year Action Plan in Beijing summer, Environ. Sci. Technol., 57, 15945–15955,

362   https://doi.org/10.1021/acs.est.3c02417, 2023.

363   Lin, Y., Zhang, Y., Fan, M, and Bao, M.: Heterogeneous formation of particulate nitrate under

364   ammonium-rich regimes during the high-PM$_{2.5}$ events in Nanjing, China, Atmos. Chem. Phys.,

365   20, 3999–4011, https://doi.org/10.5194/acp-20-3999-2020, 2020.

366   Liu, M.; Huang, X.; Song, Y.; Tang, J.; Cao, J.; Zhang, X.; Zhang, Q.; Wang, S.; Xu, T.; Kang, L.; Gai,

367   X.; Zhang, H.; Yang, F.; Wang, H.; Yu, J.; Lau, A.; He, L.; Huang, X.; Duan, L.; Ding, A.; Xue,

368   L.; Gao, J.; Liu, B.; Zhu, T. Ammonia emission control in China would mitigate haze pollution

369   and nitrogen deposition, but worsen acid rain. Proc. Natl. Acad. Sci., 116, 7760–7765,

370   https://doi.org/10.1073/pnas.1814880116, 2019.

371   Mao, I., Lin, C., Lin, C., Chen, Y., Sung, F., and Chen, M.: Exposure of acid aerosol for

372   schoolchildren in metropolitan Taipei, Atmos. Environ., 43, 5622–5629, https://doi.org/10.

373   1016/j.atmosenv.2009.07.054, 2009.

374   Masiol, M., Squizzato, S., Formenton, G., Khan, M. B., Hopke, P. K., Nenes, A., Pandis, S. N., Tositti,

375   L., Benetello, F., Visin, F., and Pavoni, B.: Hybrid multiple-site mass closure and source

376   apportionment of PM$_{2.5}$ and aerosol acidity at major cities in the Po Valley, Sci. Total Environ.,

377   704, 135287, https://doi.org/10.1016/j.scitotenv.2019.135287, 2020.

378   MEP (Ministry of Environment Protection), 2023. https://www.mee.gov.cn/ywdt/hjywnews/2024

379   06/t20240605_1075031.shtml, Accessed date:5 June 2024.

380   Nah, T., Lam, Y. H., Yang, J., and Yang, L.: Long-term trends and sensitivities of PM$_{2.5}$ pH and aerosol

381   liquid water to chemical composition changes and meteorological parameters in Hong Kong,

382   South China: Insights from 10-year records from three urban sites, Atmos. Environ., 302,

383   https://doi.org/10.1016/j.atmosenv.2023.119725, 2023.

384   Nenes, A., Pandis, S. N., Kanakidou, M., Russell, A. G., Song, S., Vasilakos, P., and Weber, R. J.:

385   Aerosol acidity and liquid water content regulate the dry deposition of inorganic reactive nitrogen,

386   Atmos. Chem. Phys., 21, 6023–6033, https://doi.org/10.5194/acp-21-6023-2021, 2021.

387   Pinder, R., Adams, P., and Pandis, S.: Ammonia emission controls as a cost-effective strategy for

388   reducing atmospheric particulate matter in the eastern United States, Environ. Sci. Technol., 41,

389   380–386, https://doi.org/10.1021/es060379a, 2007.

390   Pinder, R., Gilliland, A., and Dennis, R.: Environmental impact of atmospheric NH_3 emissions under

391   present and future conditions in the eastern United States, Geophys. Res. Lett., 35, 28,

392   https://doi.org/10.1029/2008gl033732, 2008.

393   Pye, H. O. T.; Nenes, A.; Alexander, B.; Ault, A. P.; Barth, M. C.; Clegg, S. L.; Collett Jr, J. L.; Fahey,

394   K. M.; Hennigan, C. J.; Herrmann, H.; Kanakidou, m.; Kelly, J. T.; Ku, L.; McNeill, V. F.; Riemer,

395   N.; Schaefer, T.; Shi, G.; Tilgner, A.; Walker, J.T.; Wang, T.; Weber, R.; Xing, J.; Zaveri, R. A.;

396   Zuend, A. The acidity of atmospheric particles and clouds. Atmos. Chem. Phys., 20, 4809–4888,

397   https://doi.org/10.5194/acp-20-4809-2020, 2020.

398   Rengarajan, R., Sudheer, A. K., and Sarin, M. M.: Aerosol acidity and secondary organic aerosol

399   formation during wintertime over urban environment in western India, Atmos. Environ., 45,

400   1940–1945, https://doi.org/10.1016/j.atmosenv.2011.01.026, 2011.

401   Seinfeld, J. H., Pandis, S. N., and Noone, K. J.: Atmospheric chemistry and physics: From air pollution

402   to climate change, Phys. Today., 51, 88–90, https://doi.org/10.1063/1.882420, 1998.

403   Sharma, B., Jia, S., Polana, A. J., Ahmed, M. S., Haque, R. R., Singh, S., Mao, J., and Sarkar, S.:

404   Seasonal variations in aerosol acidity and its driving factors in the eastern Indo-Gangetic Plain:

405   A quantitative analysis, Chemosphere., 305, 135490,

406   https://doi.org/10.1016/j.chemosphere.2022.135490, 2022.

407   Shi, G., Xu, J., Peng, X., Xiao, Z., Chen, K., Tian, Y., Guan, X., Feng, Y., Yu, H., Nenes, A., and Russell,

408   A. G.: pH of aerosols in a polluted atmosphere: source contributions to highly acidic aerosol,

409   Environ. Sci. Technol., 51, 4289–4296, https://doi.org/10.1021/acs.est.6b05736, 2017.

410   Shi, X., Nenes, A., Xiao, Z., Song, S., Yu, H., Shi, G., Zhao, Q., Chen, K., Feng, Y., and Russell, A.

411   G.: High-resolution data sets unravel the effects of sources and meteorological conditions on

412   nitrate and its gas-particle partitioning, Environ. Sci. Technol., 53, 3048–3057,

413   https://doi.org/10.1021/acs.est.8b06524, 2019.

414   Song, S., Nenes, A., Gao, M., Zhang, Y., Liu, P., Shao, J., Ye, D., Xu, W., Lei, L., Sun, Y., Liu, B.,

415   Wang, S., and McElroy, M. B.: Thermodynamic modeling suggests declines in water uptake and

416   acidity of inorganic aerosols in Beijing winter haze events during 2014/2015–2018/2019, Environ.

417   Sci. Technol. Lett., 6, 752–760, https://doi.org/10.1021/acs.estlett.9b00621, 2019.

418   Su, H., Cheng, Y., and Pöschl, U.: New Multiphase Chemical Processes Influencing Atmospheric

419   Aerosols, Air Quality, and Climate in the Anthropocene, Acc. Chem. Res., 53, 2034–2043,

420   https://doi.org/10.1021/acs.accounts.0c00246, 2020.

421   Surratt, J. D., Chan, A. W. H., Eddingsaas, N. C., Chan, M., Loza, C. L., Kwan, A. J., Hersey, S. P.,

422   Flagan, R. C., Wennberg, P. O., and Seinfeld, J. H.: Reactive intermediates revealed in

423   secondary organic aerosol formation from isoprene, Proc. Natl. Acad. Sci., 107, 6640–6645,

424   https://doi.org/10.1073/pnas.0911114107, 2010.

425   Tao, Y. and Murphy, J. G.: The sensitivity of $PM_{2.5}$ acidity to meteorological parameters and chemical

426   composition changes: 10-year records from six Canadian monitoring sites, Atmos. Chem. Phys.,

427   19, 9309–9320, https://doi.org/10.5194/acp-19-9309-2019, 2019.

428   Tian, Y.; Chen, G.; Wang, H.; Huang-Fu, Y.; Shi, G.; Han, B.; and Feng, Y.: Source regional

429   contributions to $PM_{2.5}$ in a megacity in China using an advanced source regional apportionment

430   method. Chemosphere., 147, 256–263, https://doi.org/10.1016/j.chemosphere.2015.12.132, 2016.

431   Tremper, A.; Font, A.; Priestman, M.; Hamad, S.; Chung, T.; Pribadi, A.; Brown, R.; Goddard, S.;

432   Grassineau, N.; Petterson, K.; Kelly, F.; Green, D.: Field and laboratory evaluation of a high time

433   resolution x-ray fluorescence instrument for determining the elemental composition of ambient

434   aerosols, Atmos. Meas. Tech., 11, 3541–3557, https://doi.org/10.5194/amt-11-3541-2018, 2018.

435   Wang, G., Chen, J., Xu, J., Yun, L., Zhang, M., Li, H., Qin, X., Deng, C., Zheng, H., Gui, H., Liu, J.,

436   and Huang, K.: Atmospheric processing at the Sea-Land interface over the South China Sea:

437   Secondary aerosol formation, aerosol acidity, and role of sea salts, J. Geophys. Res. Atmos.,

438   127, https://doi.org/10.1029/2021jd036255, 2022.

439   Wang, L., Du, H., Chen, J., Zhang, M., Huang, X., Tan, H., Kong, L., and Geng, F.: Consecutive

440   transport of anthropogenic air masses and dust storm plume: Two case events at Shanghai, China,

441   Atmos. Res., 127, 22–33, https://doi.org/10.1016/j.atmosres.2013.02.011, 2013.

442   Wang, S., Yin, S., Zhang, R., Yang, L., Zhao, Q., Zhang, L., Yan, Q., Jiang, N., and Tang, X.: Insight

443   into the formation of secondary inorganic aerosol based on high-time-resolution data during haze

444   episodes and snowfall periods in Zhengzhou, China, Sci. Total Environ., 660, 47–56,

445   https://doi.org/10.1016/j.scitotenv.2018.12.465, 2019.

446   Wang, S.; Wang, L.; Li, Y.; Wang, C.; Wang, W.; Yin, S.; Zhang, R.; Effect of ammonia on fine-particle

447   pH in agricultural regions of China: comparison between urban and rural sites, Atmos. Chem.

448   Phys., 20, 2719–2734, https://doi.org/10.5194/acp-20-2719-2020, 2020.

449   Wang, Z., Pan, X., Uno, I., Chen, X., Yamamoto, S., Zheng, H., Li, J., and Wang, Z.: Importance of

450   mineral dust and anthropogenic pollutants mixing during a long–lasting high PM event over East

451   Asia, Environ. Pollut., 234, 368–378, https://doi.org/10.1016/j.envpol.2017.11.068, 2018.

452   Weber, R.; Guo, H.; Russell, A.; Nenes, A.: High aerosol acidity despite declining atmospheric sulfate

453   concentrations over the past 15 years, Nature Geoscience., 9, 282–285,

454   https://doi.org/10.1038/ngeo2665, 2016.

455   Wei, Y.; Wang, S.; Jiang, N.; Zhang, R.; and Hao, Q. Comparative multi-model study of $PM_{2.5}$ acidity

456   trend changes in ammonia-rich regions in winter: Based on a new ammonia concentration

457   assessment method, J. Hazard., 458, 15, https://doi.org/10.1016/10.1016/j.jhazmat.2023.131970,

458   2023.

459   Wen, L., Xue, L., Wang, X., Xu, C., Chen, T., Yang, L., Wang, T., Zhang, Q., and Wang, W.:

460   Summertime fine particulate nitrate pollution in the North China Plain: increasing trends,

461   formation mechanisms and implications for control policy, Atmos. Chem. Phys., 18, 11261–

462   11275, https://doi.org/10.5194/acp-18-11261-2018, 2018.

463   Xie, Y., Wang, G., Wang, X., Chen, J., Chen, Y., Tang, G., Wang, L., Ge, S., Xue, G., Wang, Y., and

464   Gao, J.: Nitrate-dominated $PM_{2.5}$ and elevation of particle pH observed in urban Beijing during

465   the winter of 2017, Atmos. Chem. Phys., 20, 5019–5033, https://doi.org/10.5194/acp-20-5019-

466   2020, 2020.

467   Xu, K., Yin, L., Chen, Q., Liao, D., Ji, X., Zhang, K., Wu, Y., Xu, L., Li, M., Fan, X., Zhang, F., Huang,

468   Z., Chen, J., and Hong, Y.: Quantitative analysis of influencing factors to aerosol pH and its

469   responses to $PM_{2.5}$ and O_3 pollution in a coastal city, J. Environ. Sci., 151, 284–297,

470   https://doi.org/10.1016/j.jes.2024.03.044, 2025.

471   Yang, L.; Wang, S.; Duan, S.; Yan, Q.; Jiang, N.; Zhang, R.; Li, S. Characteristics and form

472   ation mechanisms of secondary inorganic ions in $PM_{2.5}$ during winter in a central city o

473   f China: Based on a high time resolution data. Atmos. Res., 233, 104696, https://doi.org

474   /10.1016/j.atmosres.2019.104696, 2019

475   Yu, F., Yan, Q., Jiang, N., Su, F., Zhang, L., Yin, S., Li, Y., Zhang, R., and Chen, L.: Tracking pollutant

476   characteristics during haze events at background site Zhongmu, Henan Province, China, Atmos.

477   Pollut. Res., 8, 64–73, https://doi.org/10.1016/j.apr.2016.07.005, 2017.

478   Zhai, S.; Jacob, DJ.; Wang, X.; Shen, L.; Li, K.; Zhang, Y.; Gui, K.; Zhao, T.; Liao, H. Fine particulate

479   matter ($PM_{2.5}$) trends in China, 2013–2018: separating contributions from anthropogenic

480   emissions and meteorology, Atmos. Chem. Phys., 19, 11031–11041, https://doi.org/10.5194/acp-

481   19-11031-2019, 2019.

482   Zhang, B., Shen, H., Liu, P., Guo, H., Hu, Y., Chen, Y., Xie, S., Xi, Z., Skipper, T. N., and Russell, A.

483   G.: Significant contrasts in aerosol acidity between China and the United States, Atmos. Chem.

484   Phys., 21, 8341–8356, https://doi.org/10.5194/acp-21-8341-2021, 2021.

485   Zhang, G., Ding, C., Jiang, X., Pan, G., Wei, X., and Sun, Y.: Chemical compositions and sources

486   contribution of atmospheric particles at a typical steel industrial urban site, Sci. Rep., 10, 7654,

487   https://doi.org/10.1038/s41598-020-64519-x, 2020.

488   Zhang, Z., Dong, Z., Zhang, C., Qian, G., and Lei, C.: The geochemical characteristics of dust material

489   and dust sources identification in northwestern China, J. Geochem. Explor., 175, 148–155,

490   https://doi.org/10.1016/j.gexplo.2016.11.006, 2017.

491   Zhang, Z., Kuang, Z., Yu, C., Wu, D., Shi, Q., Zhang, S., Wang, Z., and Liu, D.: Trans–boundary dust

492   transport of dust storms in Northern China: A study utilizing ground–based lidar network and

493   CALIPSO satellite, Remote sens.,16, 1196, https://doi.org/10.3390/rs16071196, 2024.

494   Zheng, G., Su, H., and Cheng, Y.: Revisiting the key driving processes of the decadal trend of aerosol

495   acidity in the U.S, Acs. Environ. Au., 2, 346–353, https://doi.org/10.1021/acsenvironau.1c00055,

496   2022.

497   Zheng, G., Su, H., Wang, S., Andreae, M. O., Pöschl, U., and Cheng, Y.: Multiphase buffer theory

498   explains contrasts in atmospheric aerosol acidity, Science., 369, 1374–1377,

499   https://doi.org/10.1126/science.aba3719, 2020.

500   Zhou, M., Zheng, G., Wang, H., Qiao, L., Zhu, S., Huang, D., An, J., Lou, S., Tao, S., Wang, Q., Yan,

501   R., Ma, Y., Chen, C., Cheng, Y., Su, H., and Huang, C.: Long-term trends and drivers of aerosol

502   pH in eastern China, Atmos. Chem. Phys., 22, 13833–13844, https://doi.org/10.5194/acp-22-

503   13833-2022, 2022.

504   Zhou, W., Gao, M., He, Y., Wang, Q., Xie, C., Xu, W., Zhao, J., Du, W., Qiu, Y., Lei, L., Fu, P., Wang,

505   Z., Worsnop, D. R., Zhang, Q., and Sun, Y.: Response of aerosol chemistry to clean air action in

506   Beijing, China: Insights from two-year ACSM measurements and model simulations, Environ

507   Pollut., 255, 113345, https://doi.org/10.1016/j.envpol.2019.113345, 2019.

508
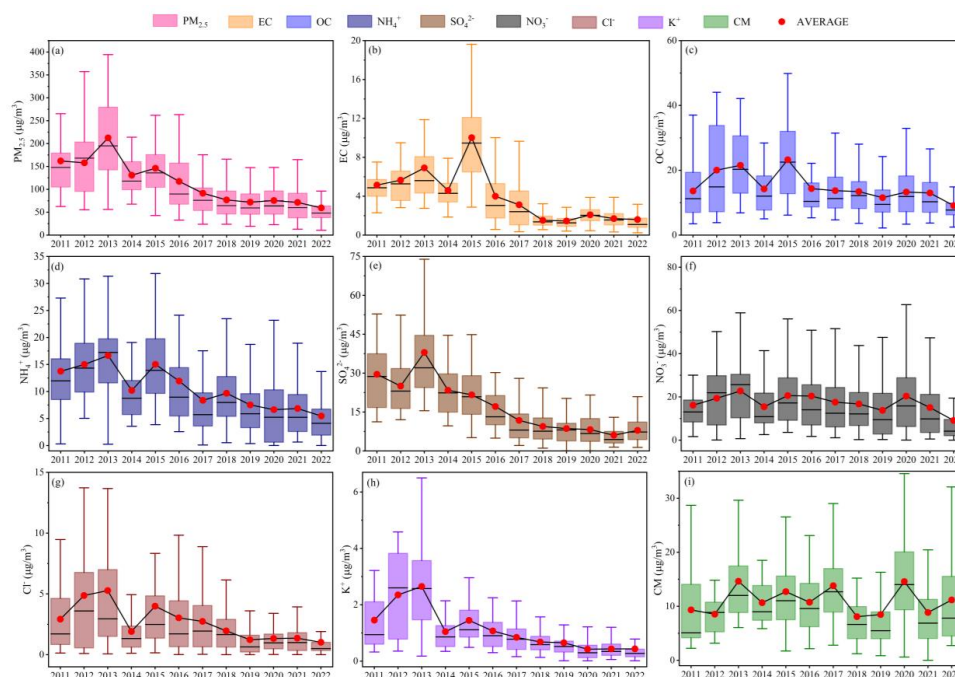
Figures

Figure 1. Long-term trends in the concentrations of PM$_{2.5}$ and its chemical components in from 2011 to 2022 in Zhengzhou. Box plots depict annual averages (red dots) and medians (black lines), the top, middle, and bottom lines represent the 75, 50, and 25 percentiles of statistical data, respectively, and the upper and lower whiskers represent the 90 and 10 percentiles of statistical data, respectively.

515
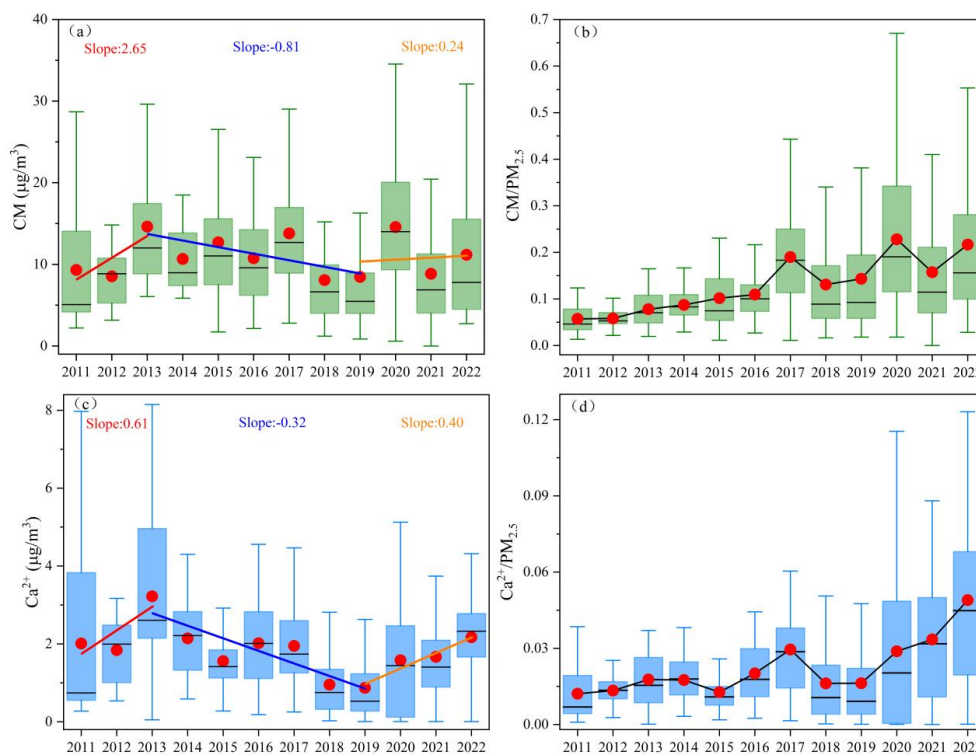
Figure 2. (a) and (c) Long-term trends in CM and Ca^{2+} concentrations in Zhengzhou from 2011 to
2022, respectively. Box plots depict annual averages (red dots) and medians (black lines), with red,
blue, and orange lines indicating annual growth rates for CM concentrations during 2011–2013,
2013–2018, and 2019–2022, respectively. (b) and (d) Long-term trends in the proportions of CM and
Ca^{2+} in $PM_{2.5}$, respectively.
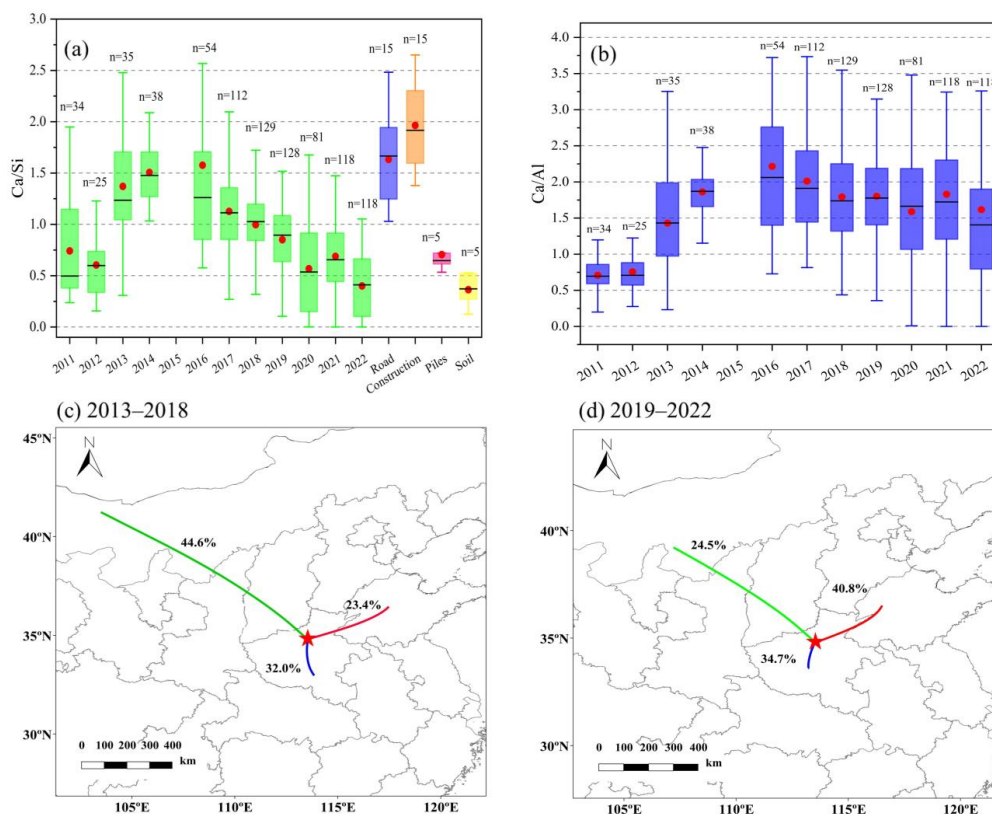
521

522 Figure 3. (a) The annual Ca/Si ratios in Zhengzhou from 2011 to 2022 compared with those in
523 various dust sources (specific values and references in Table S3). The red dots and black lines in the
524 box plots represent the annual averages and medians, respectively, with n indicating the sample size.
525 (b) The Ca/Al ratios in Zhengzhou from 2011 to 2022. The red dots and black lines in the box plots
526 represent the annual averages and medians, respectively, with n indicating the sample size. (c) and
527 (d) The transport pathways of CM during 2013–2018 and 2019–2022, respectively.

528
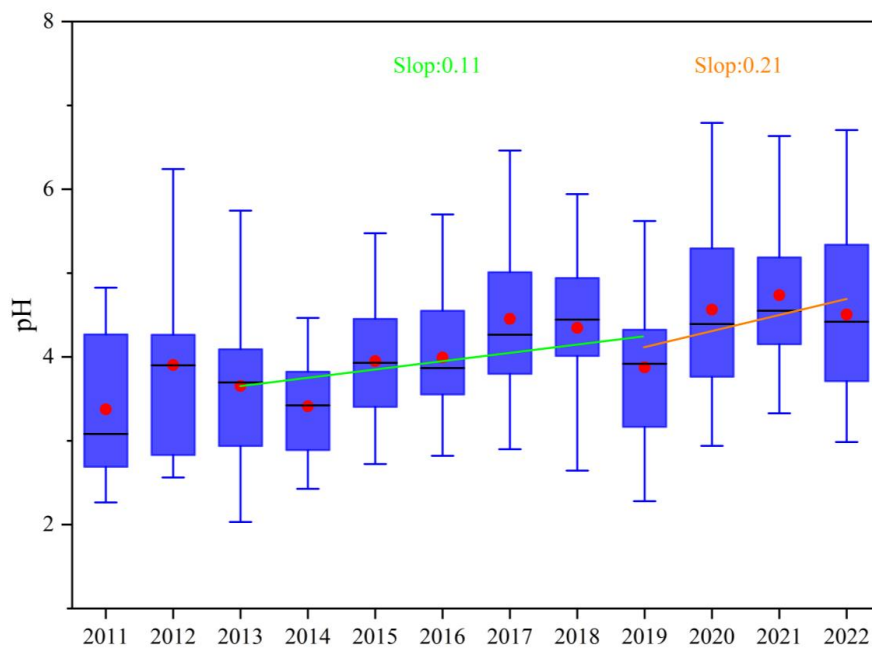
Figure 4. The time series of particle pH in Zhengzhou from 2011 to 2022. In the boxplots, red dots
and black lines represent the annual mean and median values, respectively. Green and orange lines
depict the annual average increase rates of particle pH from 2013 to 2018 and from 2019 to 2022,
respectively.

533
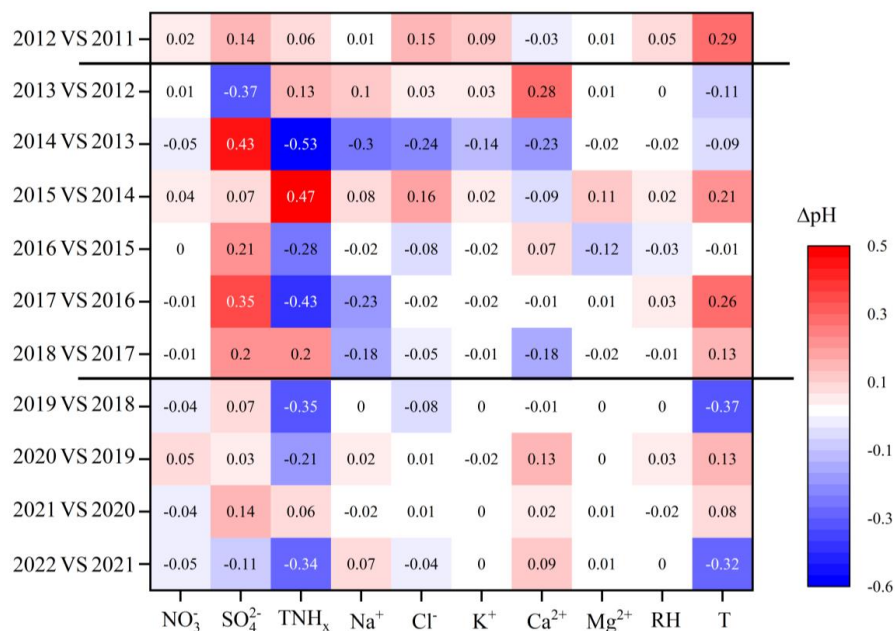
Figure 5. Contribution of each component to the changes in pH (ΔpH) between adjacent years. The
difference between component concentrations and meteorological parameters between adjacent years
is listed in Table S4.

537 **Table**

538 Table 1. Annual average concentrations of $PM_{2.5}$ and its components from 2011 to 2022 in Zhengzhou,
539 China (μg/m^3).

Years	$PM_{2.5}$	EC	OC	NO_3^-	SO_4^{2-}	NH_4^+	CM	Ca^{2+}
2011	161.9±81.4	5.1±2.1	13.6±8.6	16.2±11.2	29.6±14.3	13.8±8.3	9.3±7.3	2.0±2.2
2012	157.9±71.2	5.6±2.5	20.0±13.4	20.2±13.7	25.0±11.2	15.0±7.1	8.5±3.4	1.8±0.8
2013	212.4±101.5	6.9±3.8	21.5±10.4	22.7±13.2	38.0±19.9	17.1±6.9	14.6±8.3	3.2±2.1
2014	130.8±48.7	4.6±2.0	14.2±8.2	15.5±10.8	23.4±9.3	10.2±6.2	10.7±4.4	2.1±1.0
2015	146.1±61.0	10.0±4.7	23.2±11.6	20.6±14.5	21.6±9.8	15.7±7.5	12.7±6.8	1.6±0.7
2016	117.4±73.5	4.0±2.8	14.4±10.0	20.4±18.7	17.1±11.3	11.9±10.6	10.8±5.3	2.0±1.1
2017	91.5±61.1	3.1±2.5	13.7±7.5	17.6±15.9	11.8±11.6	8.4±7.9	13.8±6.5	2.0±1.0
2018	76.8±41.6	1.5±0.7	13.4±7.3	16.7±13.5	9.4±6.0	9.7±6.1	8.1±5.7	1.0±0.8
2019	68.4±34.8	1.5±0.8	11.5±6.8	13.8±13.9	8.6±6.4	7.5±6.1	8.5±7.8	0.9±0.9
2020	75.5±31.8	2.1±0.9	13.3±7.9	18.6±14.2	8.3±5.6	6.7±6.6	14.6±7.6	1.6±1.4
2021	71.5±45.9	1.7±0.9	13.0±8.0	15.1±15.1	6.1±4.5	6.8±6.0	8.9±7.0	1.7±1.2
2022	59.5±41.1	1.6±1.5	9.1±8.1	10.0±14.4	7.9±4.5	5.5±5.4	11.2±8.3	2.2±1.1

540